

Decay of dynamic fracturing based on three-dimensional measurements of clastic-dike geometry

Tsafrir Levi^{a,b,*}, Ram Weinberger^a, Yehuda Eyal^b

^a Geological Survey of Israel, 30 Malkhe Israel, 95501 Jerusalem, Israel

^b Department of Geological and Environmental Sciences, Ben Gurion University of the Negev, Beer Sheva, Israel

ARTICLE INFO

Article history:

Received 16 September 2008

Received in revised form

17 May 2009

Accepted 1 June 2009

Available online 10 June 2009

Keywords:

Fracture

Scaling law

Fracture tip

Dynamic fracturing

Clastic dike

ABSTRACT

Several fundamental issues of fracture mechanics during the post-dynamic stage are yet not fully understood, including fracture arrest mechanisms, effects of the three-dimensional fracture propagation on fracture aperture and height relations, and the role played by fracture tips on fracture termination. We studied these issues in the seismically active Dead Sea basin, where clastic dikes (>10 m) and numerous smaller *dikelets* (<1 m) dynamically intruded the late-Pleistocene soft rock of the Lisan Formation. A three-dimensional study of the dikelets shows that they form arrest zones at the tips of the larger clastic dikes. Geometrically, the dikelets are divided into two parts: (1) the main dikelet, in which the aperture profile along the dikelet height is approximately elliptic; and (2) the elongated tip, in which the aperture profile along the tip height is approximately constant. The dikelet aspect ratio is defined as A/H , where A is dikelet aperture and H is dikelet height. A plot of A/H versus H describes power relations with two different zones: (1) Zone A, with a small variation of A/H , between 0.02 and 0.06, for dikelets in height range of 100–700 mm; and (2) Zone B, where the aspect ratio sharply increases to 0.23 in dikelets with heights less than ~100 mm. We interpret that during deceleration, when the height of the elongated tip became greater than 1/10 of the dikelet height, inelastic conditions are dominant. Under these conditions, the fracture velocity decreases significantly and the dikelet aspect ratio increases. The present observations and analyses indicate that formation of elongated tips and dike (fracture) segmentation are essential for the decay of the dynamic fracturing.

© 2009 Elsevier Ltd. All rights reserved.

1. Introduction

The relationship between the fracture aperture and height (hereafter A – H relation) can be used to infer the mechanisms that affect the fracture growth at different length scales. The Linear Elastic Fracture Mechanics (LEFM) theory predicts a constant A – H relation (e.g., Pollard, 1987), but field observations have shown that for opening-mode fractures this relation is not necessarily applicable (e.g., Delaney and Pollard, 1981; Vermilye and Scholz, 1995). For these cases, the proposed relation is $A = cH^n$, where c is a constant, related to the material properties of the host rock, and n is a power-law exponent (Olson, 2003 and references therein). Consequently, in a case where $n < 1$ (Olson, 2003), the power of the A – H relation implies that longer fractures have smaller aspect ratios (A/H) than shorter ones.

The three-dimensional shape and size of natural fractures are not well constrained, mainly because determining precise fracture peripheries is difficult. This difficulty hinders interpreting the mechanical conditions for fracture growth. One aspect of fracture scaling is that the A – H relation for three-dimensionally analyzed fractures may be different than for the two-dimensional case (e.g., Schultz and Fossen, 2002). Hence, applying scaling laws that are based on two-dimensional fracture populations may lead to incorrect mechanical interpretations for two main reasons: (1) two individual fractures observed in plane view can coalesce to a single fracture in the third dimension (Pollard et al., 1982); and (2) hidden fracture tips may modify the A – H relation due to local stress disturbance, depending on the proximity to these tips. The latter reason leads to a non-linear A – H relation, and may increase the aspect ratio (A/H). Other aspects of fracture scaling that may lead to a non-linear A – H relation are constant fracture height due to adjacent mechanical boundaries such as bedding planes and pre-existing fractures (e.g., Helgeson and Aydin, 1991; Gross, 1993; Weinberger, 1999; Olson, 2003; Bai et al., 2000), heterogeneous (non-constant) driving pressure during fracture growth (Olson,

* Corresponding author at: Geological Survey of Israel, 30 Malkhe Israel, 95501 Jerusalem, Israel.

E-mail address: tsafir@gsi.gov.il (T. Levi).

2003), and the effect of the fracture-tip damage zone on fracture propagation (Hatton et al., 1994).

Theoretically, opening-mode fractures in elastic materials can attain velocities close to the Rayleigh wave speed (e.g., Freund, 1998). At that velocities, a branching process may create multiple secondary fractures (Sharon et al., 1996; Blumenfeld, 1998), resulting in dissipation of energy and possibly deceleration of fracture propagation. However, the mechanics of fracture deceleration and fracture geometry formed during the arresting process are not well understood (e.g., Cox et al., 2005).

To gain a better understanding of fracture propagation particularly during cessation of fracture growth, we examine the A – H relationships for clastic dikelets (<1 m in height). They are located together with large (>10 m) clastic dikes in the seismically active Dead Sea basin, where they intruded the late-Pleistocene soft rock of the Lisan Formation (Figs. 1 and 2). In previous studies, based on field observations, anisotropy of magnetic susceptibility (AMS) analysis, and optically stimulated luminescence (OSL) dating, we concluded that these dikes are injection structures that were emplaced dynamically due to fluidization of clay-rich source layers during Holocene earthquake events (Levi et al., 2006a,b; Porat et al., 2007). These studies also indicate that the injection of the fluidized

clay-rich material into the dikes occurred simultaneously with dynamic fracturing and bifurcation. Based on the turbulent channel-flow model and elastic crack theory, we showed that the injection velocity within the wider clastic dikes (≥ 0.18 m) could reach tens of meters per second, which is on the order of the dynamic fracturing velocity (Levi et al., 2008).

For this study, we took advantage of the soft rock of the Lisan Formation to dig and reveal the three-dimensional geometry of the dikelets. We showed that these dikelets form the arrest zones at the tips of the large-scale clastic dikes. Consequently, we documented the architecture of the arrest zones and constructed A – H relations of the measured dikelets. These analyses helped us to infer the decay mechanism and fracture deceleration process at the post-dynamic stage.

2. Geologic setting

The clastic dikes were studied in Ami'az Plain (Fig. 1), a down-faulted block located between the Mount Sedom salt diapir (Zak, 1967; Weinberger et al., 2006) and the western margin of the Dead Sea basin. The Dead Sea basin is associated with a transtensional segment of the Dead Sea Fault (DSF), which is an intercontinental left-lateral transform accommodating the relative motion between the African (Sinai) and Arabian plates (e.g., Quennell, 1959; Freund et al., 1968; Garfunkel, 1981).

The bedrock of Ami'az Plain is the ~40 m thick lacustrine Lisan Formation consisting mostly of authigenic aragonite laminae alternating with fine detritus layers (Fig. 2a) (Begin et al., 1980) of late-Pleistocene age (between 70,000 and 15,000 years B.P.; Haase-Schramm et al., 2004). The upper part of the Lisan Formation consists of a relatively stiff gypsum layer about 1 m thick. A thin veneer (<1 m) of eolian and fluvial sediments overlies the Lisan Formation and covers large parts of the plain. The lower part of the Lisan Formation contains several thick (<0.4 m) and stiff gypsum layers (Fig. 2a). The incision of Nahal (Wadi) Perazim in Ami'az Plain exposes the entire Lisan section, and about 250 large clastic dikes and numerous dikelets.

The paleoseismic record from the Dead Sea basin based on breccia layers in the Lisan Formation reveals numerous moderate to strong earthquake events between 70,000 and 15,000 years B.P. (e.g., Marco and Agnon, 1995; Begin et al., 2005) and during the Holocene (Enzel et al., 2000; Ken-Tor et al., 2002).

3. Sampling strategy and methods

To construct reliable A – H relations, we measured the dimensions and orientations of the dikelets by both a standard two-dimensional method (e.g., Nicholson and Pollard, 1985) and a more elaborate three-dimensional technique. The latter technique is based on exposing vertical isolated dikelet along their strike (defined here as the z -axis) by digging into the relatively soft Lisan rock in steps of 20–100 mm (Figs. 2 and 3). Measuring the apertures and the heights of the dikelets or segments and photographing their xy planes in each digging step enabled us to reconstruct the A – H relations along the strike of the dikelets. The sum of the segment dilational areas, based on the digital analysis, was calculated for each step by using the Argus software (<http://www.argusone.com/CompProfile.html>). This analysis checks if the segmentation process causes a non-linearity in the dikelet A – H relation and an increase/decrease in the A/H aspect ratios. All the dikelets studied are located away from adjacent clastic dikes and the stiff gypsum layers (Fig. 2a), and hence, they grew without mechanical disturbances from these discontinuities.

For both the two and three-dimensional methods, it is necessary to determine and measure the true dikelet height because dikelets

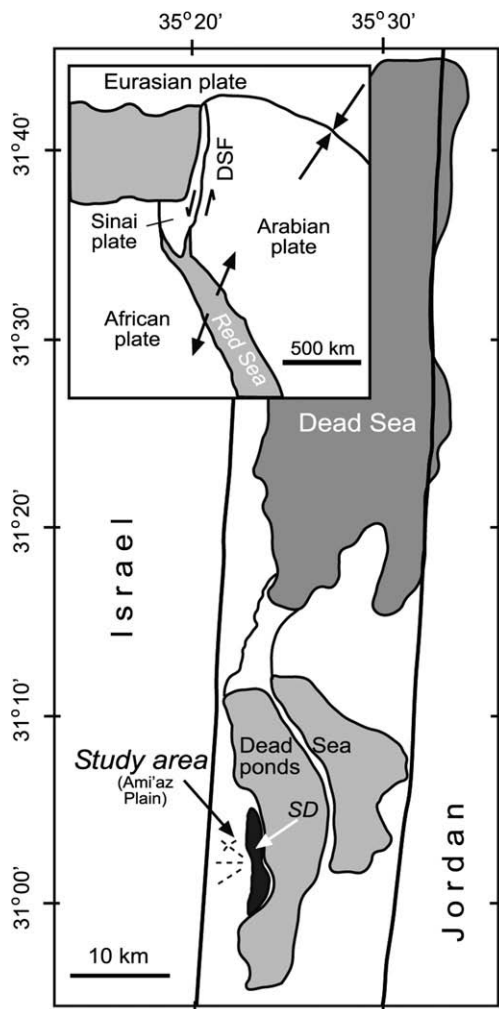


Fig. 1. Location maps of the study area. The regional setting of the Dead Sea Fault (inset), and the Ami'az Plain with the clastic dykes marked schematically by dashed lines. Solid lines represent main strands of the Dead Sea Fault (Dead Sea Fault), SD, Sedom Diapir (after Levi et al., 2006a).

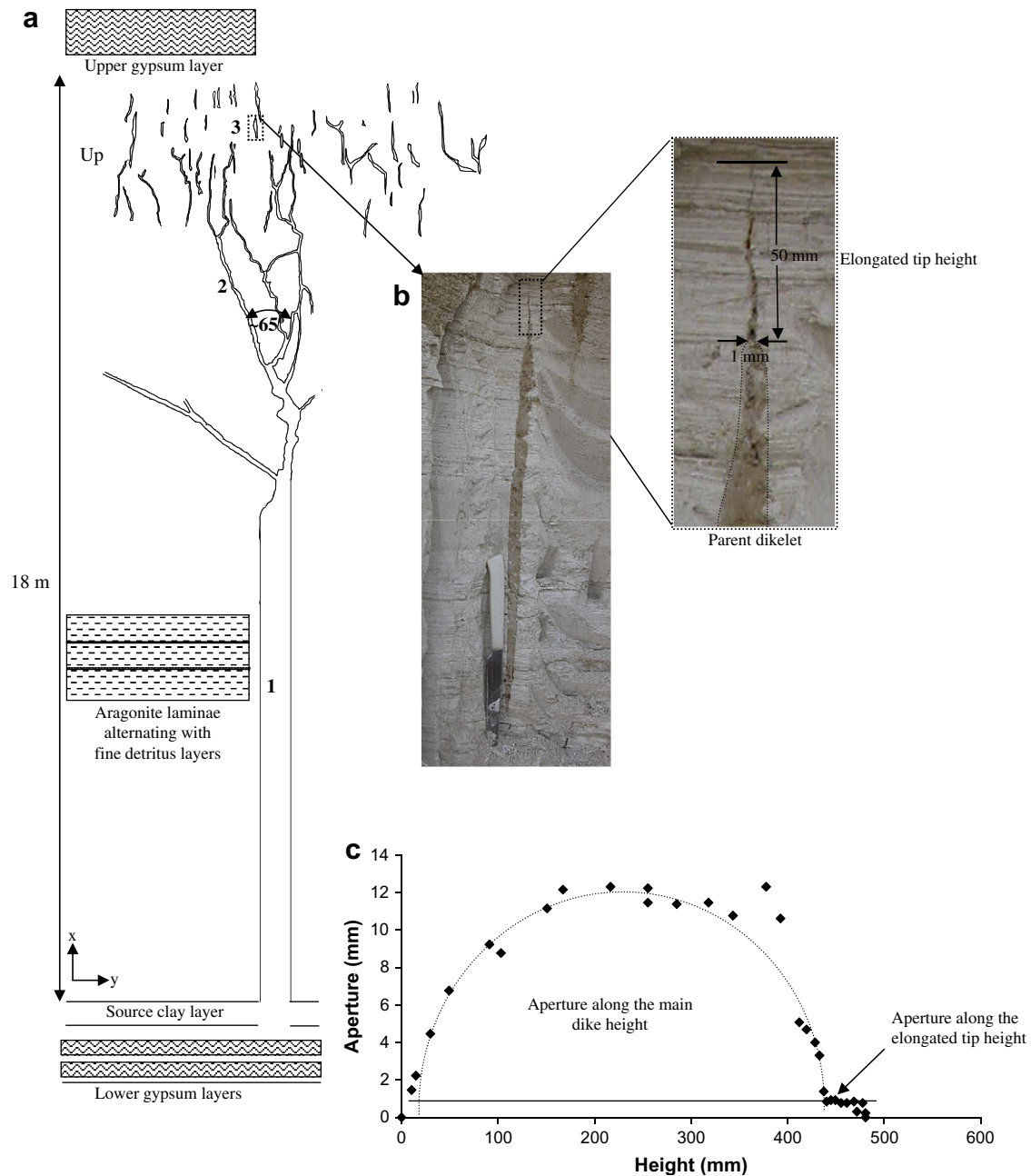


Fig. 2. (a) Vertical two-dimensional (xy plane, see Fig. 3) architecture of a clastic dike system in Ami'az Plain, Dead Sea basin. The system is divided into four sub-branching order zones (denoted by numbers) and is bordered by stiff gypsum layers. Typical angles between dike strands of the second-order zone are around 65° . The fourth-order zone consists of dikelets that formed along the strike of the third-order dikelets and cannot be seen in this view (see Fig. 3). (b) An isolated third-order dikelet and enlargement of its elongated tip. (c) $A-H$ profile of the dike in (b). The main dike is characterized by an elliptical shape, whereas the elongated tip is characterized by an almost constant aperture of ~ 1 mm.

typically have a narrow, elongated tips (Fig. 2b and c), which may introduce a bias to the height measurements. Theoretically, the aperture along a vertical profile of a dikelet should resemble an ellipse, and the aperture at its two edges is zero. Practically, dikelet edges are associated with elongated tips (Fig. 2c). Hence, to discriminate the elongated tips from the main dikelets we measured the aperture along the main dikelet height with accuracy of a tenth of a millimeter. The point at which an aperture starts to become constant is defined as the base of the tip zone and an edge of the dikelet (Fig. 2c).

Overall, two-dimensional measurements of 373 dikelets were collected from six outcrops. In addition, to check a possible genetic

linkage between dikelets and dikes, we compared a population of dikelet orientations to the orientations of 7–10 large-scale dikes that cross the same outcrops. Three-dimensional measurements of six dikelets were collected at five outcrops from the upper Lisan section.

4. Architecture of clastic-dike systems

Dike heights and apertures range from 1 mm to 20 m and 0.1 mm–200 mm, respectively. A connection between a green clay-rich layer in the lower part of the Lisan Formation and the dike-fill observed in several dikes unequivocally indicates that the clay-rich

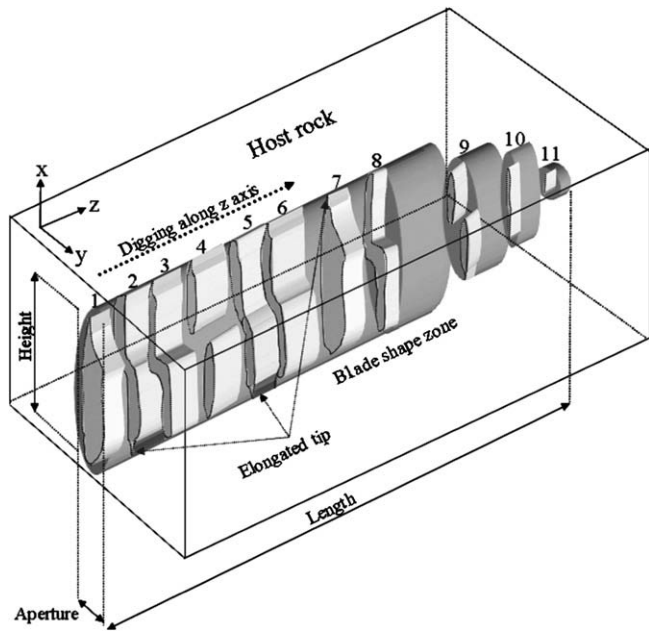


Fig. 3. A schematic three-dimensional architecture of the third- and fourth-order dikelets exposed by digging along their strike (z -axis). Note that the dikelets may split into several segments and coalesce again into a single dikelet along the strike. Numbers denoted steps in the digging along the z -axis.

layer is the source of the dikes, and the dike-fill propagated mainly upward and laterally as well as downward (Levi et al., 2006b; Porat et al., 2007). Downward, the clastic dikes terminate at the lower Lisan Formation consisting of 0.5 m stiff gypsum layers alternating with aragonite layers (Fig. 2a). Upward, the dikes either terminate against the stiff, 1 m thick, gypsum layer or cut through it to the surface. Several clastic dikes branch upward and split into several large strands (Fig. 2a), resembling the pattern of dynamic fractures that bifurcate during upward propagation (e.g., Bahat et al., 2005). We could determine four orders of branching characterized by interrelated and physically connected zones (Figs. 2 and 3). The first-order zone consists of a single parent clastic dike from which all strands and dikelets split. The second-order zone comprises 3–5 large strands about 2–7 m in height, branching from the parent dikes. The third-order zone comprises numerous dikelets (~ 0.1 –1 m high) that split from the second-order strands. Commonly, these dikelets are segmented along their strikes, forming arrays of overlapping en-echelon fractures (Fig. 3). These arrays form the fourth-order zone of dikelets (< 1 m height) at the upper part of the Lisan section, between 13 and 18 m above the clay-rich source layer. The orientation distribution of the dikelets in the third-order zone are associated with the parent clastic dikes, but with a greater orientation variability (Fig. 4). Digging laterally along the strike of the fourth-order dikelets (Fig. 3) indicated that their apertures and heights decrease so that eventually the dikelets disappear within the Lisan host rock. Several observations indicate that genetically dikelets are associated with the clastic dikes so that both are part of the same fracturing system: (1) The distribution of the dikelets and dikes is limited to the same outcrops (Fig. 2). (2) The modal orientations of the dikelets are similar to that of the neighboring large-scale dike strands (Fig. 4). In localities where two sets of dikelets were measured, similar orientations were identified for the dikes. (3) In cases where the dikes were completely exposed, physical connections between them and the dikelets were observed (Fig. 2a). (4) The sediment infill in dikes and dikelets is identical (Levi et al., 2006a,b). (5) The AMS analyses of the sediment

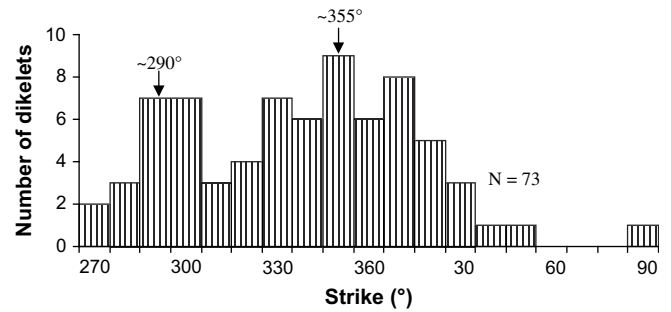


Fig. 4. (a) Histogram of 73 strikes of dikelets measured in the third-order zone. Arrows indicate the trends of two clastic dikes that cross the studied outcrop.

infill in both dikes and dikelets indicate similar flow conditions (Levi et al., 2006b).

5. Shape and A – H relations of clastic dikes

The A – H relations of 373 dikelets measured in two-dimensions are not linear and a power-law fitting is preferable (Fig. 5a). The first derivative of the power-law equation indicates that around 120 mm the slope increases sharply. Hence, dikelets that are larger than ~ 120 mm have almost constant aspect ratios (Fig. 5c and d), whereas dikelets that are smaller than that have a range of aspect ratios up to a value of 0.15 (Fig. 5d). Six dikelets that were measured in three-dimensions (Fig. 6) also show non-linear A – H relations. The aspect ratios (A/H) versus heights of four out of the six dikelets also can be characterized by a power-law relation (Fig. 6a; dikelets 'a', 'c', 'd' and 'e'). These curves reveal that the aspect ratios vary between 0.01 and 0.23 for heights < 100 mm (zone B in Fig. 6a). For heights > 100 mm (zone A), the range of aspect ratios is only between 0.02 and 0.05. For example, the heights of dikelet 'd' range between 35 and 512 mm and the slope increases sharply for dikelet smaller than 100 mm (Fig. 6b). Most of the measured heights of dikelet 'f' are greater than 90 mm and associated with aspect ratios between 0.02 and 0.06. The measured heights of dikelet 'b' show a modest range of sizes between 21 and 210 mm, whereas greater aspect ratios of up to 0.125 are related to heights of 100 mm and less. Image analysis of dikelets whose elongated tip heights could clearly be separated from the parent dikelet also supports power-law relations between the aspect ratio (A/H) and dikelet heights (Fig. 6c). From 0 to 200 mm along a single dikelet length the dilational area decreases from 5000 to 4000 mm² and increases again up to 4800 mm² (Fig. 7a). From 400 to 800 mm along the dikelet length the dilational area is almost constant (~ 3500 mm²) even though the number of the segments varies between 1 and 4. This indicates that the dilational area is not affected directly by the number of segments along the dikelet length. The aspect ratio of short segments is greater than that of longer segments and maximum values are seen at dikelet lengths of 450, 800, and 1200 mm (Fig. 8b). In cases where the dikelet terminated, the number of segments does not affect the height or aperture profile along the z -axis (Fig. 8a and b).

6. Elongated tips

The heights of the elongated tips vary between 2 and 80 mm, and the average is around 23 mm (Fig. 9a). The apertures measured at the base of the elongated tips (Fig. 10a) vary between 0.2 and 3.6 mm (average is around 0.9 mm; Fig. 9b), and typically increase with tip heights (Fig. 9c). Fig. 10 shows the geometry and relationships

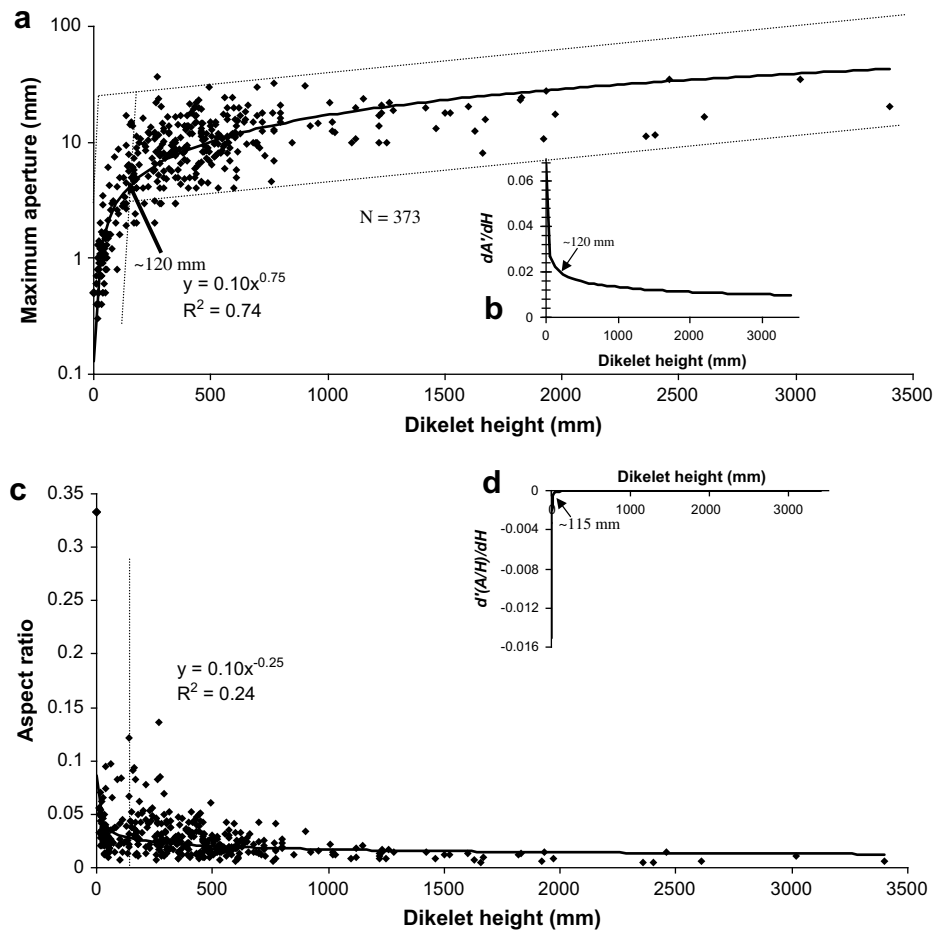


Fig. 5. (a) Maximum dikelet aperture (A) versus dikelet height (H) of 373 third-order dikelets plotted on log–linear axes. The A – H relations are that of a power-law. Pairs of dashed lines bordered the data into zones of moderate and high slopes and cross each other around 120 mm along the fitting curve. (b) First derivative curve of the power-law equation of (a) showing increase in the slope at ~ 120 mm. (c) Aspect ratios versus heights of 373 third-order dikelets plotted on linear–linear axes. (d) First derivative curve of the power-law equation of (c) showing increase in the slope at ~ 115 mm.

between dikelet tip height and aperture with respect to dikelet height. Two zones are identified in Fig. 10b: (1) Zone C, where relatively tall dikelets are associated with a large range of elongated tip heights. In this zone, the dikelet height varies between 100 and 658 mm, and the elongated tip height between 2.7 and 78 mm; (2) Zone D, where relatively short dikelets are associated with a narrow range of elongated tip heights. In this zone the dikelet height varies between 6.6 and 100 mm, and the range of the elongated tip heights is between 3 and 18 mm. Likewise, these two zones are identified in Fig. 10c: (1) Zone C has a narrow range of aspect ratios, between 0.02 and 0.06, for dikelet heights between 100 and 658 mm; (2) Zone D, which has a greater range of aspect ratios between 0.02 and 0.23 for smaller dikelet heights between 6.6 and 100 mm. The average ratio of dikelet height to elongated tip height in zone C is about 20 (~ 10 near the transition line), while the average ratio of the dikelet height to elongated tip height in zone D is about 6.

7. Discussion

Digging laterally along the strike of the fourth-order dikelets indicates that their apertures and heights decrease as the dikelets disappear within the Lisan host rock (Figs. 3 and 8). Therefore, we interpret that the branching of the parent dikes into a three-dimensional network of numerous strands and dikelets, and the segmentation of the latter along their strike represent the last stage

of the clastic-dike emplacement and termination of dynamic fracturing (Fig. 11). Field data of dynamic fracturing systems is scant, and data of laboratory experiments (e.g., Yoffe, 1951; Ravi-Chandar and Knauss, 1984; Sharon et al., 1996; Ravi-Chandar, 1998; Sagy et al., 2001) is limited to the sample scale. In the Ami'az Plain study area, where the clastic dikes propagated through an “infinite” medium, the architecture of a dynamic fracturing system and their associated arrest zones is well exposed and can be studied in three-dimensions to yield insight into fracture cessation.

7.1. A – H relation

Several arguments indicate that during the dike emplacement the Lisan host rock behaved in a brittle manner and like a linear elastic material. The clastic dikes are filled fractures with smooth wall planes that sharply crosscut the Lisan rock. Small-scale faulting and tilting of Lisan lamellae were observed within an overlapping zone between two dike/dikelet segments. On the other hand, indications of ductile deformation such as viscous fingering between the injected slurry and the Lisan rock are absent.

The Lisan was deposited in an aqueous environment, and ductile deformation of the soft sediments occurred close to deposition as evidenced by tight synsedimentary folds. However, OSL ages of dike emplacement suggest that many dikes intruded

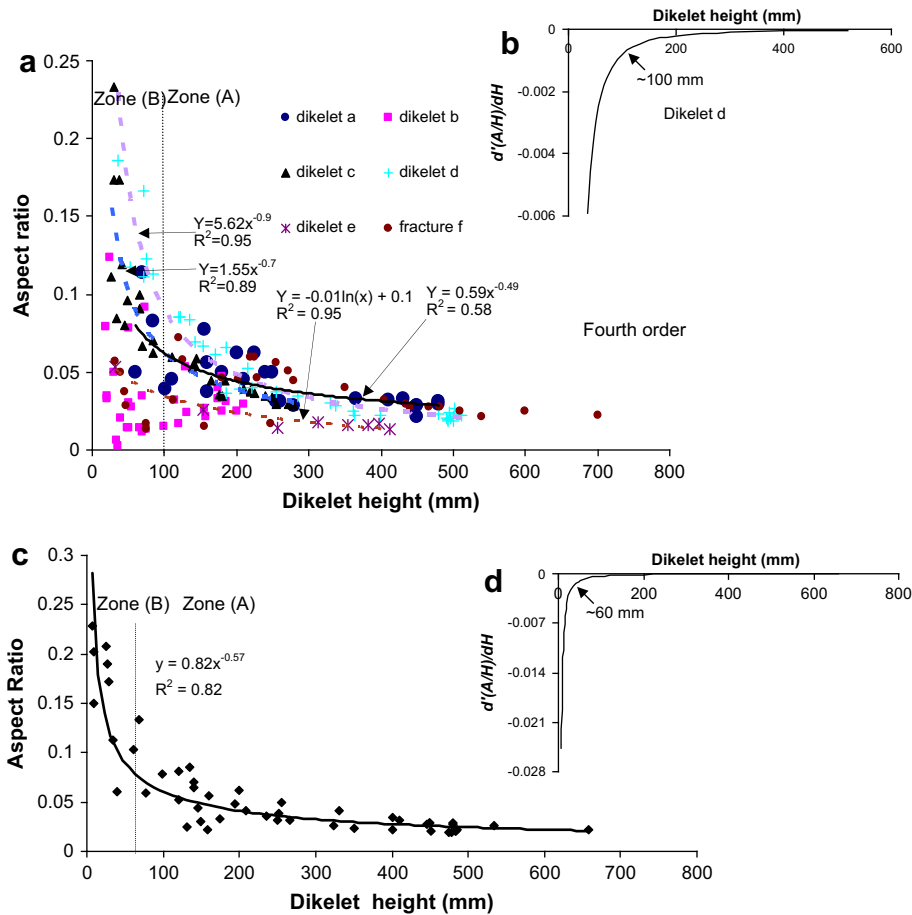


Fig. 6. (a) Aspect ratios versus heights of six dikelets from the fourth-order zone that were measured in three-dimensions and plotted on linear axes. Fitting power-law curves for four of the dikelets are marked with different colors. The vertical dotted line divides the data into two zones of different aspect ratios. See text for details. (b) First derivative curve of the power-law equation of (a) for dikelet "d" showing increase in the slope at ~ 100 mm. (c) Aspect ratio versus dikelet height for fourth-order dikelets that were analyzed digitally along the z-axis. The vertical dotted line divides the data into two zones of different aspect ratios. See text for details. (d) First derivative curve of the power-law equation of (c) showing increase in the slope at ~ 60 mm.

the Lisan host rock after a significant drop in the Lake Lisan water level (Porat et al., 2007). Hence, it is likely that the Lisan rocks lost a significant amount of moisture before fracturing and their properties were similar to those at present. By analyzing the dikelets geometry, we showed that most dikelets have an elliptical shape, suggesting that the dikelets were dilated elastically (Levi et al., 2008). Therefore, it is likely that brittle fracturing and elastic deformation were dominant during dike emplacement, and hence, the dikelet $A-H$ relations can be discussed in terms of the elastic theory.

We explored the $A-H$ relations of the dikelets because characterization dynamic fracturing behavior by dikelet orientations alone is not conclusive (Fig. 4). A power-law scaling of the dikelet $A-H$ relation and aspect ratio adequately represents both two and three-dimensional fracture populations (Figs. 5 and 6). Based on the analysis of the power-law relations (Figs. 6 and 10), two zones can be distinguished: (1) The zone in which the aspect ratio varies in a narrow range (zone A, Fig. 6a and c) for dikelets whose height varies between 100 and 700 mm. The almost constant aspect ratio in this zone indicates that the dimensions of the dikelet aperture and height were achieved at an almost constant driving pressure (ΔP_0) as predicted from linear elastic fracture mechanics (LEFM) (e.g., Delaney and Pollard, 1981);

where M is the elastic stiffness of the host rock; and (2) The zone in which the aspect ratio is not constant (zone B; Fig. 6a and c) for the range of dikelet heights between 7 and 100 mm. Because the aspect ratio is not constant in this zone, Equation (1) is not applicable and inelastic processes around the dikelet tips became dominant. The number of segments did not affect the total dilational area of the blade-like dikelets along their z-axis. Hence, during the segmentation process the amount of injected material through an individual blade-like dike and its associated segments/dikelets did not vary significantly. However, the heights of the segments are smaller than that of their parent dike (Fig. 7b), resulting in relatively greater aspect ratios of the third- and fourth-order dikelets. Large aspect ratios formed when the segments became relatively small and close to their end (Fig. 8), indicating the importance of the segmentation process in the post-dynamic stage and dike termination. During this stage, the dikelet $A-H$ relation is not constant and depends on the height of the elongated tip (Fig. 10).

7.2. The association between the dikelet $A-H$ relations and the size of the elongation tip under arrest conditions

The termination of the dikelets is the expression of a deceleration stage, in which the fracturing velocity decreased to zero.

$$A/H = \Delta P_0/M, \quad (1)$$

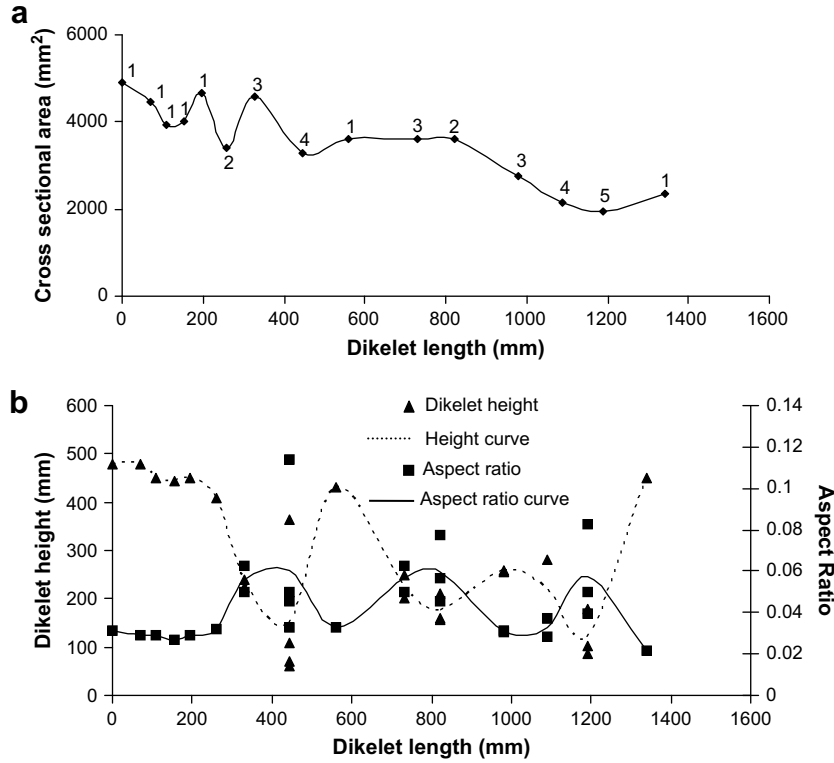


Fig. 7. (a) Total dilational area along the length of dikelet 'a' calculated by summing segment dilational areas in digital images of xy planes (see definition in Fig. 2). Diamonds represent the exposed localities by step-digging along the z-axis. The number of segments observed at each step is indicated. (b) Variations in the segment heights and calculated aspect ratios along the z-axis. The dash and solid lines connect the average values of the heights and aspect ratios, respectively.

Hence, the initial dynamic (accelerated) propagation of the clastic dikes was changed at final stages to propagation under deceleration conditions (Fig. 11), up to termination of the fracturing. In that sense, the present study differs from most published works (e.g.,

Rubin, 1993) in which the dike (fracture) geometry is assumed to be the expression of growing conditions, either under constant or accelerating velocities.

The dikelets have a typical narrow elongated tip at the front of their edges. In zone C, the elongated tip heights are not constant even for the same dikelet sizes (Fig. 10b). This geometry applies for single dikelets with one (Fig. 2b) or two elongated tips and for the entire population of dikelets that have different elongated tip heights. The variable elongated tip heights in zone C can be explained in four ways. First, two elongated tips with different sizes may develop at single dikelet edges. The dilation profile of the pressure-driven fractures (dikes) is composed of three parts, namely, the elliptical shape, the teardrop shape, and the diamond shape (Delaney and Pollard, 1981). Levi et al. (2008) analyzed the dilation profile of the dikelets based on the elastic theory and showed that they mainly dilate into an elliptical shape by the uniform component of the driving pressure (ΔP_0) (Levi et al., 2008). Nevertheless, a best-fit analysis indicates that the dilation profile of the dikelets slightly deviates from the perfect elliptical shape and includes components of teardrop and diamond shapes. This geometry implies that on the dikelet edges, different magnitudes of linear stress gradients existed, forming elongated tips with different sizes.

Second, the Lisan Formation is apparently characterized by contrasting material properties of alternating aragonite and fine detritus layers that have different resistance to fracturing. Furthermore, the thickness of the bounding detritus layers might control the dikelet and the elongated tip propagation (e.g., Rijken and Cooke, 2001). However, the height variations due to this possibility seem to be minor, because field observations indicate that most elongated tips belonging to single dikelets propagated in similar set of alternating aragonite and fine detritus layers. Third,

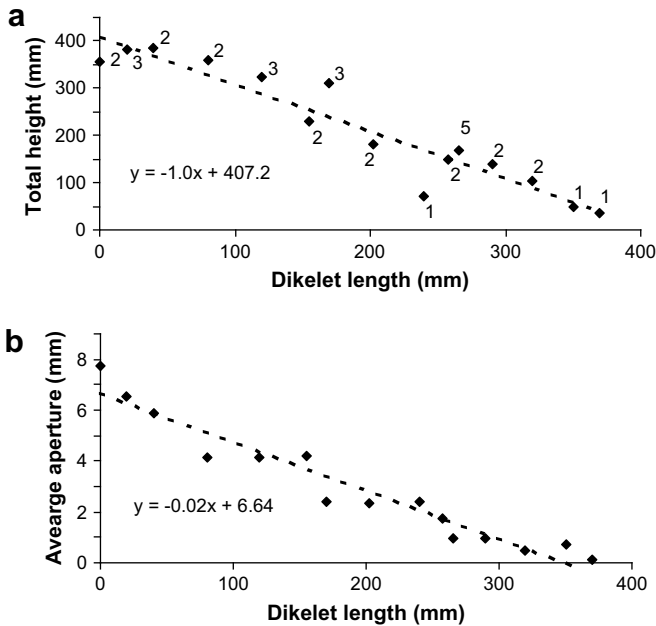


Fig. 8. Changes in total height (a) and average aperture (b) relative to decreasing length of dikelet 'b' up to termination. The number of segments observed at each step and linear regression lines fitted to the data are presented.

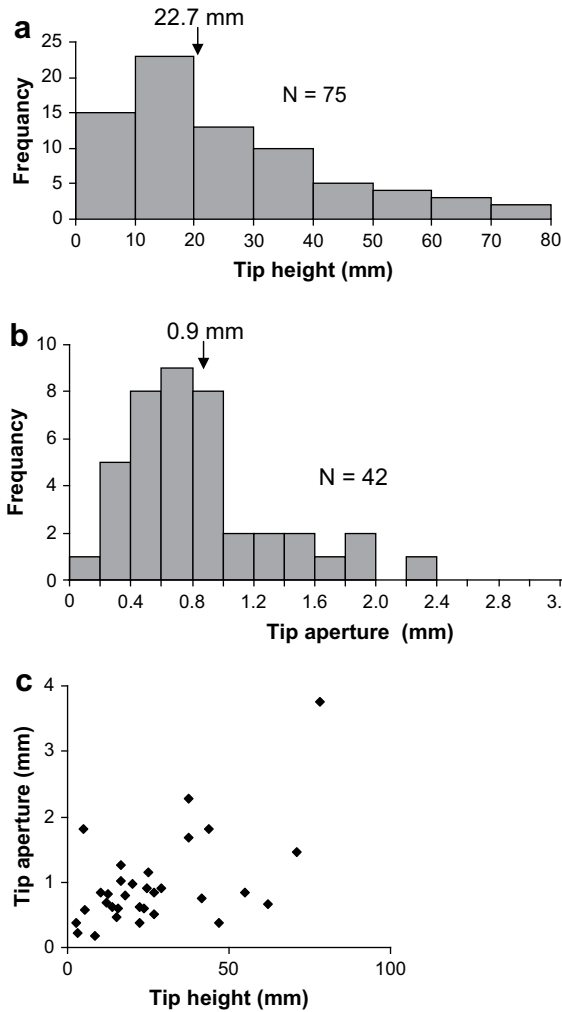


Fig. 9. Frequencies of (a) height and (b) aperture of elongated tips. The apertures were measured in the base of the elongated tips (Fig. 2c) and are equal to the crack tip opening displacement (CTOD). Arrows indicate the mean height and aperture of elongated tips. The number of heights is greater than the number of apertures because the apertures of the elongated tips were measured only in cases where the base of this zone was clear. (c) Apertures of elongated tips versus their height.

under deceleration conditions, the dikelets reduced their apertures and heights along the z -axis. Hence, different heights (2a) of the main dikelets formed along the z -axis may result in different stress intensities (K_I) at their edges,

$$K_I = \Delta P_0 (\pi a)^{0.5} \quad (2)$$

Assuming that ΔP_0 is equal in all dikelets due to their interrelated physical connection suggests different elongated tip height, R_y ,

$$R_y = 0.5a(\Delta P_0/\sigma_{YS})^2, \quad (3)$$

where σ_{YS} is the yielding stress (Anderson, 1995 and references therein). Yet, this explanation is less probable, because there is no linear correlation between the height of the main dikelet and the height of the elongated tip (Fig. 10b).

Fourth, during tip interaction the closure stress at the segment tips may vary between pairs of overlapping segments (e.g., Bai et al., 2000). This variation may lead to changes in the size of the

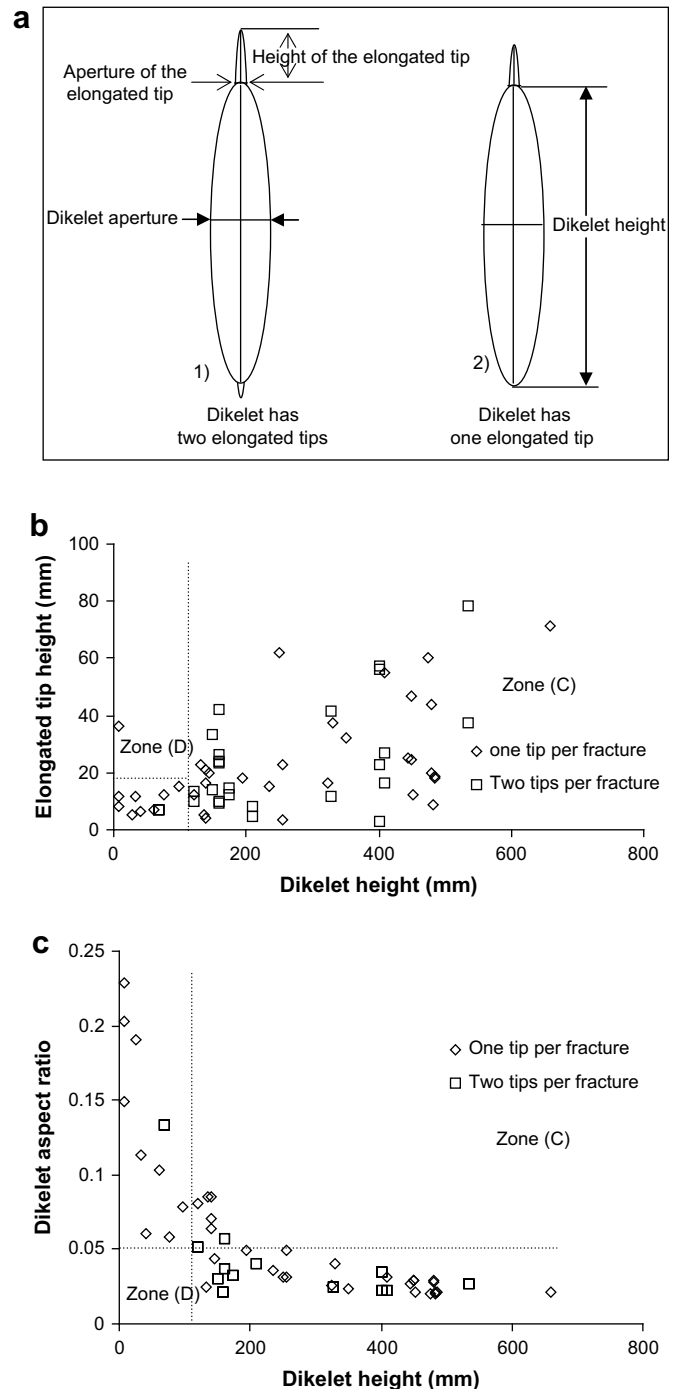


Fig. 10. (a) Schematic showing the geometry and definitions of dikelet and tip dimensions. (b) Relations between the heights of the elongated tips and their parent dikelet plotted on linear axes. (c) Relations between the aspect ratio of the dikelets and the dikelet heights plotted on linear axes.

elongated tip and formation of segment (dikelet) populations that have different tip heights. However, segment interaction would also change the dikelet aspect ratio (Olson, 2003), yet it varies in a narrow range in zone C (Fig. 10c), suggesting that the interaction between segments was not dominant. Therefore, we suggest that the above first explanation is the main reason for the observed variations in the elongated tip height, but the relative importance of this and the other explanations should be further studied.

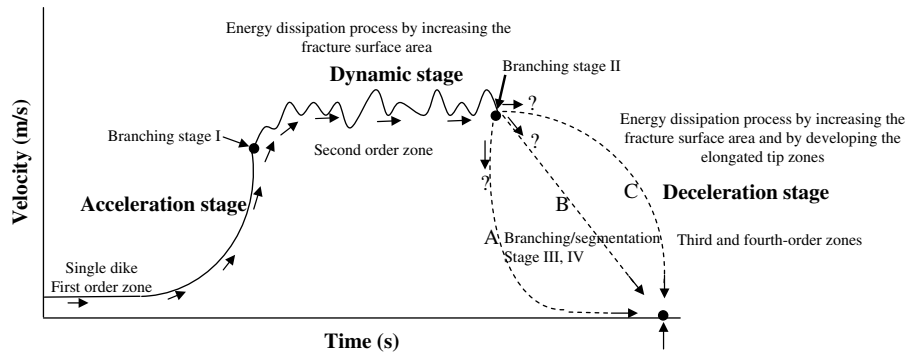


Fig. 11. A model of the evolution of dynamic fracturing with time. At the first stage the accelerated velocity is associated with a single dike. The first branching that forms the second-order zone occurs during minor oscillations of the velocity. The third- and the fourth-order zones (the dikelets) develop during velocity deceleration. The dash lines represent alternative paths (A, B, and C) for the deceleration with time. Because in the “arrest zone” (fourth-order zone) the fracture velocity decreased sharply (see Fig. 11) path A is preferable.

7.3. Elongated tip heights and fracture velocities

A bunch of three-dimensional dikelets belonging to the same dike and injection system and connected to the same source layer are interpreted to be formed in a single event (Levi et al., 2006b). In addition, in zones A and C all dikelet populations indicate an almost constant aspect ratio, suggesting that during the propagation and injection of the dike-fill the driving pressure (ΔP_0) was almost constant (Equation (1)). Assuming constant driving pressure for dikes with different heights implies variations in the stress intensity K_I (Equation (2)). High stress intensity magnitudes are associated with high fracture velocities, because fracture velocity V depends on the stress intensity, $V \propto K_I^n$ (n is material-dependent) (e.g., Anderson, 1995; Weinberger and Bahat, 2008). On the other hand, under quasi-static and arrest conditions, the stress intensity factor should be equal or lower than the fracture toughness (K_{IC}) (Anderson, 1995, p. 219–223), otherwise the fracture propagation will never stop.

In zone A or C LEFM is verified, allowing the use of Equation (2) for estimating the stress intensity magnitudes. Using the variables in Table 1 for dikelet height of 0.02 m, results in a stress intensity of about 1 MPa m^{0.5}. This value is more than one order of magnitude larger than the fracture toughness of soft rock (Table 1).

At a certain point, the elongated tip height becomes more than 1/10 of the dikelet height (zone B or zone D; Figs. 6 and 10), and inelastic processes are dominant. Consequently, the stress intensity may be estimated under the Elastic–Plastic condition (Anderson, 1995),

$$K_I = \left(\frac{\delta \sigma_{YS} E}{1 + 1/6 \left(\frac{\pi \Delta P_0}{2 \sigma_{YS}} \right)^2} \right)^{0.5}, \tag{4}$$

where E is the Young modulus, and δ is the crack tip opening displacement (CTOD) (Anderson, 1995) δ is equal to the aperture of the elongated tip (along the x -axis). Using Equation (4) and inserting the variables from Table 1, the calculated stress intensities are equal or less than 0.1 MPa m^{0.5}. This value is of the same order as the fracture toughness of the soft rock, and is also at least one order of magnitude smaller than the calculated stress intensity for zone A. Consequently, the dikelet height becomes shorter due to the lower stress intensities, while the dikelet aperture is relatively wide, resulting in greater aspect ratios. Hence, the relative enlargement of the elongated tip height is associated with a reduction of the stress intensity magnitudes and, consequently, a decrease in the associated fracture velocity.

The above scenario also provides insights into the dikelet segmentation process (Fig. 12). During this process, the dikelet aspect ratios increase (Figs. 7b and 12), implying that the stress intensity and fracture velocity for each segment (dikelet) decreased. Hence, the more a dikelet is segmented, the lower the fracture velocity of each segment (Fig. 12). In cases where the segment is less than 0.1 m, it would be terminated at a short distance, which would make the parent dike shorter as well. In the next step, the dikelet would be segmented again and the same process may occur. Hence, the segmentation process along the dikelet length might reduce the high fracture velocity attained during the dynamic fracturing. It is also accompanied by an increase of fracture surfaces and energy dissipation (Pollard et al., 1982).

Both elongated tip zones and process zones are similar in the sense that they are small zones, either along the fracture plane (elongated tip) or out-of-plane (process zone), near the end of the fracture in which all non-linear and dissipative fracture processes occurs. Development of elongated tips or process zones at the front of the main fracture can result in dissipation of fracturing energy. The fracture process zone, which accompanies a dynamically propagating crack, plays a crucial role in determining the dynamics

Table 1
Values of variables of soft rock used for calculations.

Variable	Symbol	Values	Source
Dikelet half height	H	0.05–2 m	field observations
Dikelet aperture	A	2–20 mm	field observations
CTOD	δ	0.2–3.5 mm	field observations
Driving pressure	ΔP_0	2–4 MPa	Levi et al. (2008)
Poisson's ratio	$\nu_{elastic}$	0.4	Gee-Clough et al., 1994; Vallejo and Lobo-Guerrero, 2002; Chetrit, 2004; Othman, 2005; Bala et al., 2006
Shear modulus	μ	50–100 MPa	Gannon et al., 1999; Schneider et al., 1999; Yuan-qiang and Xu, 2004; Chetrit, 2004; Bala et al., 2006
Young modulus	E	100–300 MPa	Chetrit, 2004
Tensile strength	T	0.1 MPa	Arkin and Michaeli, 1986
Fracture toughness	K_{IC}	0.03–0.1 MPa m ^{0.5}	Delaney and Pollard, 1981; Spence and Turcotte, 1985; Zhang, 2002; Chen and Zhang, 2004; Funatsu et al., 2004
Yielding stress	σ_{YS}	0.4 MPa	Karig, 1996

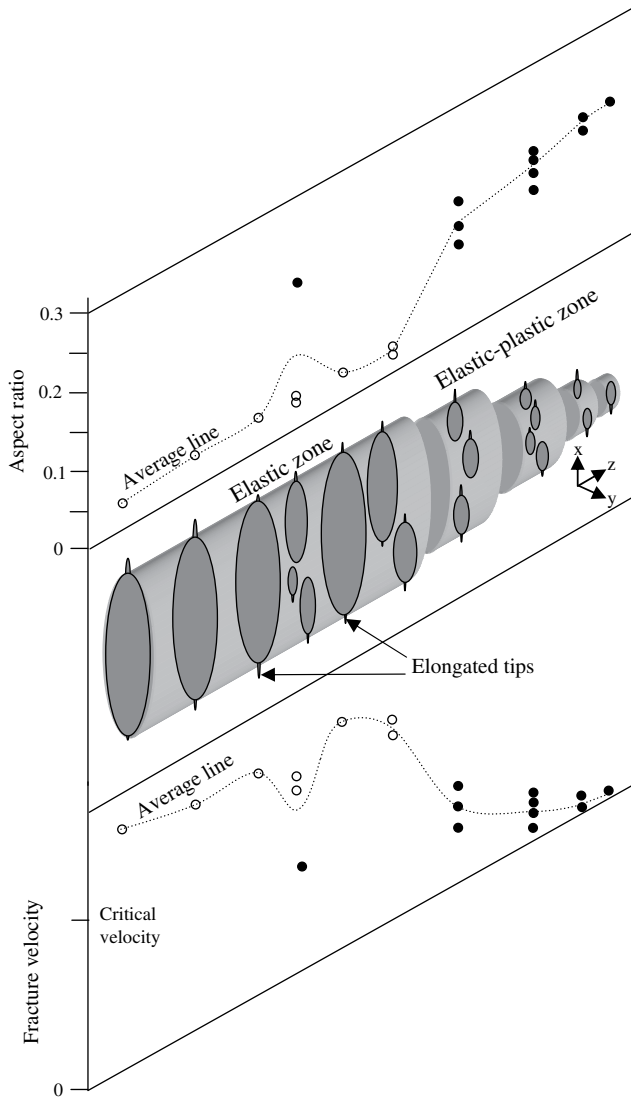


Fig. 12. A schematic, three-dimensional model describing the development of a dikelet arrest zone at the post-dynamic stage. In the blade-like dikelet, the height of the segments (parent dikelet) (xy plane) is ten times (or more) greater than the height of the elongated tip, in accordance with the elastic condition and the constant aspect ratio. Different segment sizes result in small variations of fracture velocity. In the elastic–plastic zone the height of the segments is only ten times (or less) longer than the elongated tip height indicated for an inelastic condition. The inelastic condition sharply reduces the fracture velocity and the dikelet height and increases the aspect ratio values. Open circles mark the segments that are ten times (or more) greater than the elongated tip height, and filled circles mark only the segments that are less than ten times greater than the elongated tip height. A critical fracture velocity is achieved when $K_I = K_{Ic}$.

of crack growth, including the limiting of fracture velocity (Biegel et al., 2008) and branching (Yang and Ravi-Chandar, 1996).

8. Conclusions

- 1) The dikelets form a unique zone that express a deceleration stage of dynamic fracturing. In that sense, the present study differs from most published works in which the fracture geometry is assumed to be the expression of growing conditions, either under constant or accelerated velocities.
- 2) A power-law scaling of the dikelet A – H relation and aspect ratio adequately represents both two and three-dimensional fracture populations.

- 3) Contrary to the LEFM prediction, in propagation during a single event, the ratio between the fracture (dike) height and its elongated tip height is not constant.
- 4) During the post-dynamic stage, when the dikelet height becomes less than ten times the height of the elongated tip, the inelastic process becomes dominant; this is also expressed by a non-linear behavior of the A – H relation and variations in the dikelet aspect ratio.
- 5) The segmentation process plays a major role during the post-dynamic stage, forming numerous dikelets. It reduces the height of the dikelet to a critical size, and, consequently, the velocity is sharply decreased.
- 6) Elongated tips in the third- and especially fourth-order dikelets are well developed. The formation of the elongated tips multiplied by the segmentation process may lead to increase in the total energy dissipation during the termination stage of the dynamic fracturing.

Acknowledgments

This study was supported by a grant from the Israeli Ministry of National Infrastructures. We are indebted to the Editor, William M. Dunne, and Michele Cooke and Ashely Griffith for their thorough and very helpful reviews. Discussions with Shmuel Marco and Vladimir Lyakhovsky are highly acknowledged, as well as the field assistance of Moshe Arnon and Yaacov Rafael.

References

- Anderson, T.L., 1995. Fracture Mechanics, Fundamentals and Applications, second ed. CRC Press, Inc, USA, p. 688.
- Arkin, Y., Michaeli, L., 1986. The significance of shear strength in the deformation of laminated sediments in the Dead Sea area. *Israel Journal of Earth Sciences* 35, 61–72.
- Bahat, D., Rabinovitch, A., Frid, V., 2005. Tensile Fracturing in Rocks. Springer-Verlag, Berlin, p. 557.
- Bai, T., Pollard, D.D., Gross, M.R., 2000. Mechanical prediction of fracture aperture in layered rocks. *Journal of Geophysical Research B: Solid Earth* 105 (1), 707–721.
- Bala, A., Raileanu, V., Zihan, I., Ciugudean, Viorica, Grecu, B., 2006. Physical and dynamic properties of the shallow sedimentary rocks in the Bucharest Metropolitan area. *Romanian Reports in Physics* 58 (2), 221–250.
- Begin, Z.B., Nathan, Y., Ehrlich, A., 1980. Stratigraphy and facies distribution in the Lisan formation—new evidence from the area south of the Dead Sea, Israel. *Israel Journal of Earth Sciences* 29, 182–189.
- Begin, Z.B., Louie, J.N., Marco, S., Ben-Avraham, Z., 2005. Prehistoric Seismic Basin Effects in the Dead Sea Pull-apart: the Ministry of National Infrastructures Geological Survey of Israel Report GSI/04/05, p. 31.
- Biegel, R.L., Sammis, C.G., Rosakis, A.J., 2008. An experimental study of the effect of off-fault damage on the velocity of a slip pulse. *Journal of Geophysical Research* 113. doi:10.1029/2007JB005234.
- Blumenfeld, R., 1998. Dynamics of fracture propagation in the mesoscale: theory. *Theoretical and Applied Fracture Mechanics* 30, 209–223.
- Chen, M., Zhang, G.-Q., 2004. Laboratory measurement and interpretation of the fracture toughness of formation rocks at great depth. *Journal of Petroleum Science and Engineering* 41, 221–231.
- Chetrit, M., 2004. Subsurface Structure at the NW Coast of the Dead Sea – a Geophysical Study. M.Sc. thesis, Ben-Gurion University of the Negev, p. 66 (in Hebrew, English abstract).
- Cox, B.N., Gao, H., Gross, D., Rittel, D., 2005. Modern topics and challenges in dynamic fracture. *Journal of the Mechanics and Physics of Solids* 53, 565–596.
- Delaney, P.T., Pollard, D.D., 1981. Deformation of host rocks and flow of magma during growth of mintette dikes and breccia-bearing intrusions near Ship Rock, New Mexico. U.S. Geology Survey Professional Paper, 1202, pp. 1–61.
- Enzel, Y., Kadan, G., Eyal, Y., 2000. Holocene earthquakes inferred from a fan-delta sequence in the Dead Sea graben. *Quaternary Research* 53, 34–48.
- Freund, L.B., 1998. Dynamic Fracture Mechanics. Cambridge University Press, Cambridge, p. 581.
- Freund, R., Zak, I., Garfunkel, Z., 1968. Age and rate of sinistral movement along the Dead Sea Rift. *Nature* 220, 253–255.
- Funatsu, T., Setob, M., Shimada, H., Matsui, K., Kuruppu, M., 2004. Combined effects of increasing temperature and confining pressure on the fracture toughness of clay bearing rocks. *International Journal of Rock Mechanics and Mining Sciences* 41, 927–938.
- Gannon, J.A., Masterton, G.G.T., Wallace, W.A., Wood, D.M., 1999. Piled foundations in weak rock. Reprinted in 2004 (London), Sharing Knowledge Building Best Practice, CIRIA Report, p. 37.

- Garfunkel, Z., 1981. Internal structure of the Dead Sea leaky transform in relation to plate kinematics. *Tectonophysics* 80, 81–108.
- Gee-Clough, D., Wang, J., Kanok-Nukulchai, 1994. Deformation and failure in wet clay soil: part 3, finite element analysis of cutting of wet clay by tines. *Journal of Agricultural Engineering Research* 58, 121–131.
- Gross, M.R., 1993. The origin and spacing of cross joints: examples from Monterey Formation, Santa Barbara coastline, California. *Journal of Structural Geology* 15, 737–751.
- Haase-Schramm, A., Goldstein, S.L., Stein, M., 2004. U–Th dating of Lake Lisan aragonite (late Pleistocene Dead Sea) and implications for glacial East Mediterranean climate change. *Geochimica et Cosmochimica Acta* 68, 985–1005.
- Hatton, C.G., Main, I.G., Meredith, P.G., 1994. Non-universal scaling of fracture length and opening displacement. *Nature* 367, 160–162.
- Helgeson, D.E., Aydin, A., 1991. Characteristics of joint propagation across layer interfaces in sedimentary rocks. *Journal of Structural Geology* 13, 897–911.
- Karig, D.E., 1996. Uniaxial reconsolidation tests on porous sediments: mudstones from site 8971. In: Whitmarsh, R.B., Sawyer, D.S., Klaus, A., Masson, D.G. (Eds.), *Proceedings of the ODP, Scientific Results. Ocean Drilling Program, vol. 149*, pp. 363–373.
- Ken-Tor, R., Agnon, A., Enzel, Y., Stein, M., Marco, S., Negendank, J.F.W., 2002. High-resolution geological record of historic earthquakes in the Dead Sea basin. *Journal of Geophysical Research* 106, 2221–2234.
- Levi, T., Weinberger, R., Aifa, T., Eyal, Y., Marco, S., 2006a. Earthquake-induced clastic dikes detected by anisotropy of magnetic susceptibility. *Geology* 34, 69–72. doi:10.1130/G-22001.1.
- Levi, T., Weinberger, R., Aifa, T., Eyal, Y., Marco, S., 2006b. Injection mechanism of clay-rich sediments into dikes during earthquakes. *Geochemistry Geophysics Geosystems* 7 (2), 1–20. doi:10.1029/2006GC001410. Q12009.
- Levi, Weinberger, R., Eyal, Y., Lyakhovsky, V., Heifetz, E., 2008. Velocities and driving pressures of clay-rich sediments injected into clastic dikes during earthquakes. *Geophysical Journal International* 175, 1095–1107.
- Marco, S., Agnon, A., 1995. Prehistoric earthquake deformation near Masada, Dead Sea graben. *Geology* 23, 695–698.
- Nicholson, R., Pollard, D.D., 1985. Dilation and linkage of echelon cracks. *Journal of Structural Geology* 7, 583–590.
- Olson, J.E., 2003. Sublinear scaling of fracture aperture versus length: an exception or rule? *Journal of Geophysical Research* 108 (B9), 1–11. ETG 3.
- Othman, A.A.A., 2005. Construed geotechnical characteristics of foundation beds by seismic measurements. *Journal of Geophysics and Engineering* 2, 126–138.
- Pollard, D.D., 1987. Elementary fracture mechanics applied to the structural interpretation of dykes. In: Halls, H.C., Fahrig, W.F. (Eds.), *Mafic Dyke Swarms. Geological Society of Canada, Special Paper*, vol. 34, pp. 5–24.
- Pollard, D.D., Segall, P., Delaney, P.T., 1982. Formation and interpretation of dilatant echelon cracks. *Geological Society of America Bulletin* 93, 1291–1303.
- Porat, N., Levi, T., Weinberger, R., 2007. Possible resetting of quartz OSL signals during earthquakes—evidence from late Pleistocene injection dikes, Dead Sea basin, Israel. *Quaternary Geochronology* 2, 272–277.
- Quennell, A.M., 1959. Tectonics of the Dead Sea Rift. In: 20th International Geological Congress, pp. 385–405.
- Ravi-Chandar, K., 1998. Dynamic fracture of nominally brittle materials. *International Journal of Fracture* 90, 83–102.
- Ravi-Chandar, K., Knauss, W.G., 1984. An experimental investigation into dynamic fracture: I. Crack initiation and arrest. *International Journal of Fracture* 25, 247–262.
- Rijken, P., Cooke, M.L., 2001. Role of shale thickness on vertical connectivity of fractures: application of crack-bridging theory to the Austin Chalk, Texas. *Tectonophysics* 337, 117–133.
- Rubin, A.M., 1993. Tensile fracture of rock at high confining pressure: implications for dike propagation. *Journal of Geophysical Research* 98, 15919–15935.
- Sagy, A., Reches, Z., Roman, I., 2001. Dynamic fracturing: field and experimental observations. *Journal of Structural Geology* 23, 1223–1239.
- Schneider, J.A., Hoyos Jr., L., Mayne, P.W., Macari, E.J., Rix, G.J., 1999. Field and Laboratory Measurements of Dynamic Shear Modulus of Piedmont Residual Soils. *Behavioral Characteristics of Residual Soils, GSP 92*. ASCE, Reston, VA, pp. 12–25.
- Schultz, R.A., Fossen, H., 2002. Displacement–length scaling in three dimensions: the importance of aspect ratio and application to deformation bands. *Journal of Structural Geology* 24, 1389–1411.
- Sharon, E., Gross, S.P., Fineberg, J., 1996. Energy dissipation in dynamic fracture. *Physical Review Letters* 76, 2117–2120.
- Spence, D.A., Turcotte, D.L., 1985. Magma-driven propagation of cracks. *Journal of Geophysical Research* 90, 575–580.
- Vallejo, L.E., Lobo-Guerrero, S., 2002. The elastic moduli of soils with dispersed oversize. In: 15th ASCE Engineering Mechanics Conference June 2–5, 2002, Columbia University, New York, NY.
- Vermilye, J.M., Scholz, C.H., 1995. Relation between vein length and aperture. *Journal of Structural Geology* 17, 423–434.
- Weinberger, R., 1999. Initiation and growth of cracks during desiccation of stratified muddy sediments. *Journal of Structural Geology* 21, 379–386.
- Weinberger, R., Bahat, D., 2008. Relative fracture velocities based on fundamental characteristics of joint-surface morphology. *Terra Nova* 20, 68–73.
- Weinberger, R., Lyakhovsky, V., Baer, G., Begin, Z.B., 2006. Mechanical modeling and InSAR measurements of Mount Sedom uplift, Dead Sea Basin: implications for rock-salt properties and diapir emplacement mechanism. *Geochemistry Geophysics Geosystems* 7. doi:10.1029/2005GC001185 Q05014.
- Yang, B., Ravi-Chandar, 1996. On the role of the process zone in dynamic fracture. *Journal of Mechanics and Physics of Solids* 44 (12), 1955–1976.
- Yoffe, E.H., 1951. The moving griffith crack. *Philosophical Magazine* 42, 739–750.
- Yuan-qiang, C., Xu, L., 2004. Dynamic properties of composite cemented clay. *Journal of Zhejiang University Science* 5 (3), 309–316.
- Zak, I., 1967. *The Geology of Mount Sedom*. Ph.D. thesis, Hebrew University, Jerusalem.
- Zhang, Z.X., 2002. An empirical relation between mode I fracture toughness and the tensile strength of rock. *International Journal of Rock Mechanics and Mining Sciences* 39, 401–406.